

See discussions, stats, and author profiles for this publication at: <https://www.researchgate.net/publication/268870764>

Facile Synthesis of Highly Stable and Water-Soluble Magnetic MWCNT/ α -Fe Nanocomposites

ARTICLE *in* THE JOURNAL OF PHYSICAL CHEMISTRY C · NOVEMBER 2014

Impact Factor: 4.77 · DOI: 10.1021/jp5077142

CITATIONS

2

READS

85

4 AUTHORS, INCLUDING:



[Barbara Malgorzata Maciejewska](#)

Adam Mickiewicz University/NanoBioMedical ...

4 PUBLICATIONS 10 CITATIONS

[SEE PROFILE](#)



[Emerson Coy](#)

Adam Mickiewicz University

21 PUBLICATIONS 28 CITATIONS

[SEE PROFILE](#)



[Krzysztof Kozioł](#)

University of Cambridge

125 PUBLICATIONS 1,961 CITATIONS

[SEE PROFILE](#)

Facile Synthesis of Highly Stable and Water-Soluble Magnetic MWCNT/ α -Fe Nanocomposites

Barbara M. Maciejewska,^{*,†,‡} L. Emerson Coy,[†] Krzysztof K. Koziol,[§] and Stefan Jurga^{†,‡}

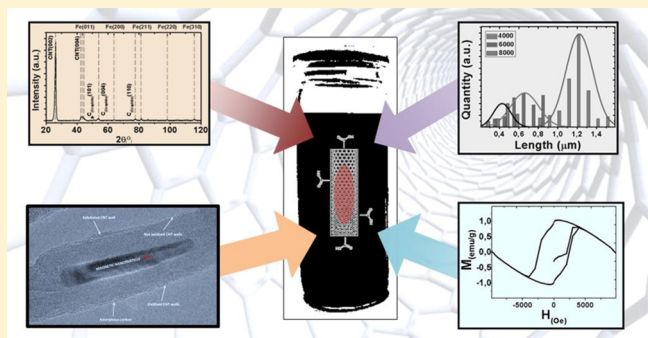
[†]NanoBioMedical Centre, Adam Mickiewicz University, Umultowska 85, 61-614 Poznan, Poland

[‡]Department of Macromolecular Physics, Faculty of Physics, Adam Mickiewicz University Umultowska 85, 61-614 Poznan, Poland

[§]Department of Materials Science and Metallurgy, University of Cambridge, 27 Charles Babbage Road, Cambridge CB3 0FS, U.K.

Supporting Information

ABSTRACT: Multiwall carbon nanotubes (MWCNT) were synthesized by the floating catalyst chemical vapor deposition (FCCVD) method. As a result, nanotubes containing metallic iron (α -Fe) were obtained and characterized. The impact of surface modification, on MWCNTs stability in water, was thoroughly studied applying three oxidative protocols. Samples were further characterized and correlated based on scanning electron microscopy (SEM), high resolution transmission electron microscopy (HR-TEM), Raman spectroscopy, Fourier transform infrared spectroscopy (FT-IR), X-ray diffraction (XRD), and thermal gravimetric analysis (TGA), and the magnetic nature of the embedded nanoparticles was assessed by means of a SQUID magnetometer at room temperature in powder. Finally, precise length segregation of MWCNT/ α -Fe nanocomposites was achieved. The studied structures showed excellent quality and unmatched stability in water after more than three months.



INTRODUCTION

Carbon nanotubes (CNT) are a class of materials undergoing rapid development in recent years. They have attracted a strong interest, mainly due to their extraordinary physical and chemical properties, such as high electrical conductivity and stiffness.¹ A promising material with potential applications in electronics, aerospace, and biomedical applications^{2,3} still generates complex questions in contemporary science; for instance, can CNT be incorporated into the human body and used as a potential drug delivery system as well as magnetic resonance contrast agents?⁴ Toxicity of these materials is under intensive debate.⁵ Many studies indicate that the biocompatibility of CNT is influenced by their size, purity, method of synthesis, and functionalization.⁶ Moreover, studies have shown a relationship between toxicity and length of multiwall carbon nanotubes (MWCNT).^{7,8} This phenomenon is attributed to the needle-like shape of MWCNT which allows them to penetrate the cell membrane without leading to apoptosis.^{9,10} However, other studies have reported contradictory results¹¹ showing the absence of consensus in this matter.

An important advantage of MWCNT related to medical applications relies on the possibility of encapsulation of magnetic particles within MWCNT, even during the synthesis procedure. This possibility makes them a perfect candidate for theranostic applications which combines treatments and diagnosis in a single multifunctional particle. However, a further important aspect concerning the use of these structures in medicine is their poor solubility in most organic solvents. As-

prepared, not functionalized, MWCNT are hydrophobic¹² which results in a low interaction with polar environment; thus, a very low biocompatibility is observed. Enhancing the chemical reactivity of the outer walls of MWCNT facilitates the attachment of various chemical groups to the outer surface of tubes.

The preparation and functionalization method, as well as the purity of MWCNT, are crucial factors that influence the properties and the interaction with other materials.¹³ One of the challenges is to develop a synthesis and functionalization protocol that would allow to obtain reproducible, controllable, and high quality CNT samples, giving a much needed ground for a consensus in their applications and properties.

On the other hand, magnetic nanoparticles are a promising material for imaging and multimodal applications;¹⁴ in specific, iron-based nanoparticles are used to improve the so-called negative MRI contrast, which provides a more detailed imaging response, sensibility, and effectiveness.¹⁵ Iron particles can be functionalized or encapsulated in diverse structures in order to improve biocompatibility and imaging response.¹⁶ Negative MRI contrast (created mostly by iron oxide particles or iron particles) is induced by local magnetic field disturbance of atom nuclei in their closest surrounding (most common hydrogen nuclei).¹⁷ It results in more effective nuclei relaxation process

Received: July 31, 2014

Revised: October 29, 2014

Published: November 5, 2014



and better differentiation of tissue elements in specified regions. However, a common problem of these particles is the low magnetic moment observed that ultimately limit the applicability of such structures.¹⁸

Iron nanoparticles are typically kept under 30 nm in order to make them safe for cellular uptake;¹⁶ moreover, at this size range, particles are superparamagnetic. The possibility of keeping magnetic particles safe from environmental degradation while preserving their functional properties intact is an important challenge that can be solved by developing MWCNT's/magnetic nanocomposites.^{19,20}

Carbon nanotubes with less than 1 wt % Fe²¹ and 2.21 wt % Fe²² content have shown improved MRI contrast capabilities; however, iron oxide–MWCNT composites have shown better performance in various studies.^{23,24} Composites of carbon nanotubes and magnetic particles are typically prepared in ex-situ procedures.^{23–25} The advantages of such preparation method are unknown, while the limitation of such synthesis method can be easily appreciated. Ex-situ procedures allow contamination of samples and rely on random events of functional conjugation without effectively forming composites; moreover, the particles attached to the nanotubes lack of adhesion and depend on weak interactions to keep them in place, leading to potential environmental and health issues. However, such studies have shown promising results in magnetic resonance imaging CNT's²⁶ and MWCNT's,^{22,24,27} driving an increasing attention to such composites and, moreover, reinforcing the need of efficient and reliable synthesis methods of such functional nanocomposites.

In this paper, we report the synthesis of MWCNT by means of floating catalyst chemical vapor deposition method (FCCVD). In this way, ferromagnetic particles are directly introduced inside on the MWCNT, giving them enhanced protection from ionic liquids and degradation. Moreover, synthesized particles present room temperature ferromagnetism due to the shape anisotropy effect of the internal conducts of the nanotubes. Samples of MWCNT were synthesized using different ferrocene concentrations, and the influence of the catalyst on the quality and morphology of the MWCNT is discussed. Finally, we introduce and discuss three different optimized protocols of CNT oxidation in order to address their stability in polar solvents in longer periods of storage that ultimately will prevent further degradation and agglomeration due to magnetic or other effects.

EXPERIMENTAL DETAILS

CVD Synthesis. The floating catalyst CVD method, described elsewhere,^{28,29} was used to synthesize MWCNT carpets. The synthesis was run in a horizontal reactor at the temperature of 760 °C under an argon atmosphere. Three different amounts of ferrocene were used as catalysts: 2, 5, and 10 wt %. During the synthesis, the rest of the growth parameters were kept constant. Samples were collected, weighted, and stored in sterile conditions.

Functionalization Protocols. The generally acknowledged mixture of sulfuric acid and nitric acid was used as functionalization mechanism.³⁰ Samples were placed in a flask with a 3:1 ratio mixture of sulfuric (98%) to nitric acid (70%); concentration was standardized to be around 0.1 wt % as shown in Figure 1.

Sonication. After 24 h of acid treatment in a sonication bath at temperature of >45 °C and power 200 W, the mixture of the acid and MWCNT was filtrated using plenty of deionized

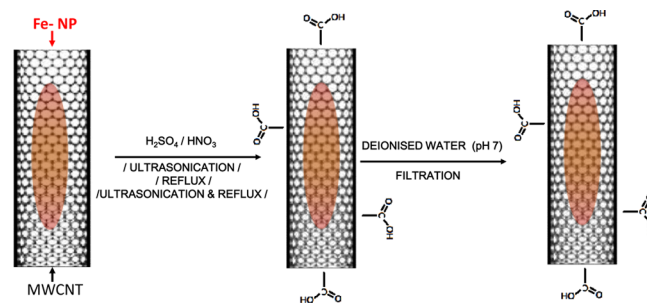


Figure 1. Three protocols of the oxidation and cutting process of MWCNT: sonication, reflux, and sonication and reflux.

water (19 Ω). The PTFE filters were used to cleanse of oxidized MWCNT (O-MWCNT) until the pH was neutral. After the procedure MWCNT containing carboxyl and carbonyl groups were obtained and redispersed in water solution.

Reflux. During the reflux treatment the mixture of acids and the MWCNT were heated up to 120 °C in a round-bottom flask attached to a condenser. The vapors were continuously condensing for reboiling for period of 15 min. The time of reflux process has been measured since the first reflux drop appeared.

Sonication and Reflux. Prior to the reflux treatment, the washed mixture of the acids and the MWCNT was kept in the water-filled ultrasonic bath (temperature >45 °C, power 200 W) for 3 h; subsequently, the solution was heated up to 120 °C in a round-bottom flask attached to the reflux condenser. The vapors were continuously condensed and reboiled for 15 min. The filtrating procedure was repeated as for treatments described before in this text.

Characterization. Morphological characterization was performed by scanning electron microscopy (SEM Jeol 7001TTL) and transmission electron microscopy (HRTEM Jeol ARM 200F). Raman spectra were obtained using a Raman spectrometer (Ramascope-1000) with a laser wavelength of $\lambda = 633$ nm. Data were collected using four accumulations of 10 s each. X-ray diffractometer working with Cu source was used to investigate the crystalline composition of the carpets and the Fe nanoparticles. Fourier transform infrared (FTIR) absorption measurements were carried out using a Bruker IFS 66/s spectrometer in the wavenumber range 1000–4500 cm⁻¹ with a resolution of 4 cm⁻¹. Prior to measurement MWCNT were mixed with potassium bromide (KBr) and then compressed into a thin pellet and measured at atmospheric pressure. Thermal gravimetric analysis (TGA) studies were performed by heating up the samples to 1000 °C with rate of 10 °C/min. Finally, the magnetic nature of the embedded nanoparticles was assessed by means of a SQUID magnetometer at room temperature in powder.

Separation. A technique of differential centrifugation was used to separate the O-MWCNT suspensions into different fractions with a narrow length distribution. The length separation of the O-MWCNT dispersed in deionized water was accomplished using Eppendorf MiniSpin microcentrifuge. The amount of 0.2 mg of O-MWCNT was dispersed in 20 mL of deionized water and ultrasonicated for 30 min. Obtained solution was centrifuged for 95 min using 4000 rpm speed. Thereafter, two different phases appeared and were placed into separate Eppendorf vials. The solution was then centrifuged at a higher rpm (for this example, 6000 rpm), and the sediments

were filled up with deionized water and centrifuged again for 95 min using a speed of 8000 rpm. This procedure was repeated with increasing speed up to the point in which no sediments were detectable. Typically no detectable sediments were present in floating solutions above 10 000 rpm (depends on the tube size).

RESULTS AND DISCUSSION

As-Prepared Samples. The stabilized iron phase was investigated by X-ray diffraction (Figure 2). The results show

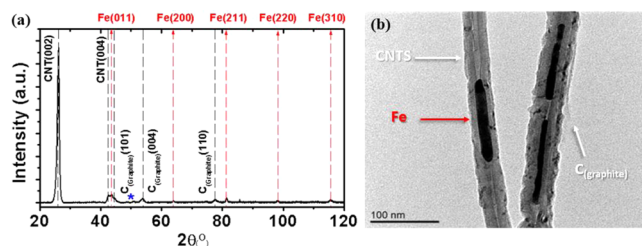


Figure 2. (a) X-ray diffractometry of as-prepared 5 wt % MWCNT powder. The distinctive sets of reflections for α -Fe are observed. (b) The origin of each of the observed groups, with the C (graphite) peaks attributed a pseudo-peeling effect on the MWCNT.

weak but conclusive features of α -Fe (ferrite), iron carbide species as well as some small secondary phases of graphite, attributed to a peeling-like effect of the MWCNT. The morphology and quality of the as-prepared MWCNT carpets were verified using scanning electron microscopy and transmission electron microscopy. Images of the as-prepared MWCNT carpets with three different catalyst contents used during the FCCVD synthesis are presented in Figure 3. Obtained MWCNT are clearly aligned. TEM images revealed that nanotubes grown with different catalyst concentration

contain an embedded metallic nanoparticles. It was also observed that such feature was present in every nanotube and would appear several times at random different lengths. As expected, the longer the nanotubes, the more particles are trapped in their central cavity.

The influence of catalyst content in the morphological properties of MWCNT has been previously discussed in the literature, and different growth mechanisms have been proposed as responsible for the filling and morphology of CNT, IE base and tip growth,^{29,31–33} and later on a combination of both.³⁴ The combined mechanism is often observed in filled nanotubes^{32,35,36} and is the one that can be expected in the floating catalyst method, in particular in the nanocomposite of MWCNT/ α -Fe. In order to understand the role of catalyst content on the MWCNT, a statistical analysis of the obtained nanotubes was performed by recording different parameters such as CNT thickness and Np diameter and length. Data were collected from 100 individual measurements of MWCNT and iron Np for different catalyst concentrations of 2, 5, and 10 wt % and represented on histograms (Figure 3d). MWCNT size distribution histograms show three distinctive distributions. MWCNT synthesized with 2 wt % show a normal distribution centered around 30 nm with a fwhm of \approx 9 nm; 5 wt % has a distribution centered around 50 nm with a fwhm of \approx 8.5. Finally, MWCNT synthesized at 10 wt % show a distribution centered \approx 41 nm and a fwhm \approx 23 nm. Data collected for nanoparticle thickness (Figure 3e) indicate no distinct difference between various catalyst concentrations. The mean particle size is calculated as \approx 18 nm. Filling percentage (F) is tabulated as the ratio between $F = Np_L/Np_T$, where Np_L stands for particle length and Np_T for particle thickness. This approach was used in order to clearly observe the dispersion of sizes above pseudo-spherical particles of each sample concentration. Extracted values were tabulated

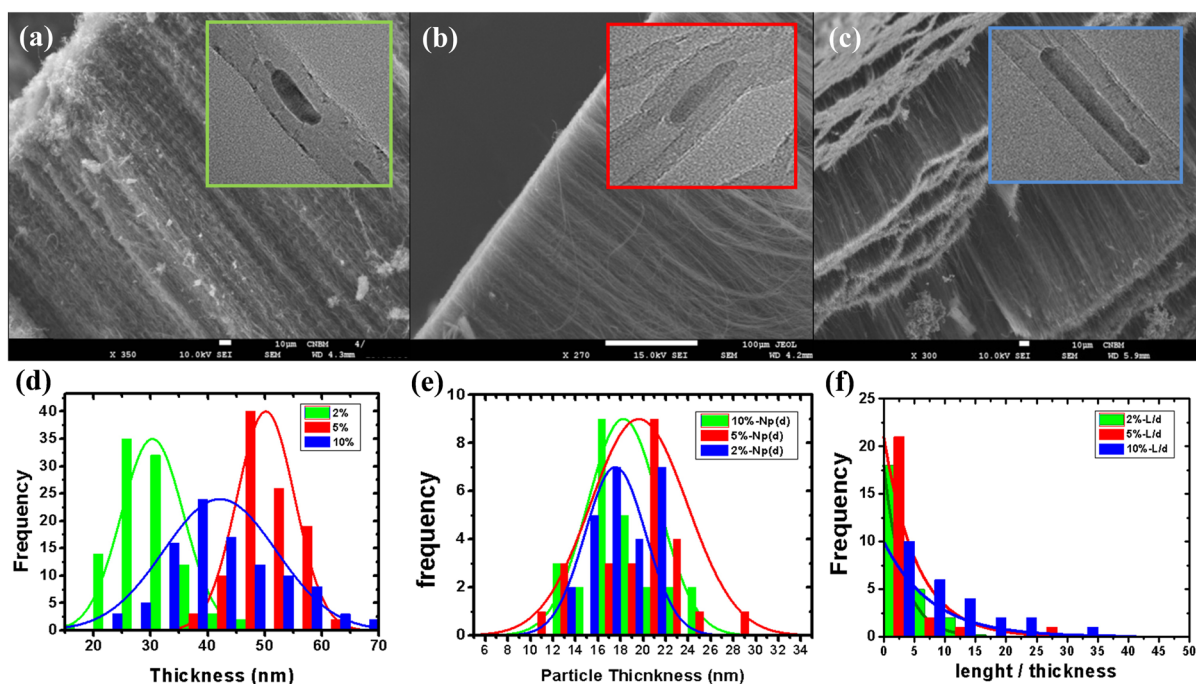


Figure 3. SEM scans of as-prepared MWCNT carpets made by FCCVD using (a) 2, (b) 5, and (c) 10 wt % of catalyst. Insets show a typical HRTEM image of a particle embedded in a MWCNT. (d) Histogram of CNT thicknesses by catalyst concentration. (e) NPs size distribution. (f) NPs ratio between thickness and length.

and presented in the histogram shown in Figure 3f, following a negative exponential distribution, with mean values of 3.58, 2.43, and 6.15 and variance of 9.45, 28.11, and 57.87 for 2, 5, and 10 wt %, respectively.

The collected information strongly suggest a direct relationship between the catalyst concentration and nanotube thickness, as observed in other studies,³² with the higher values of catalyst giving a broad dispersion of nanotube thicknesses. Interestingly enough, particle diameter has no visible correlation with catalyst concentration showing that the thickness increment is related to the nanotube graphitic layer and walls and not related to the seeding particle. Nanotube filling, on the other hand, shows direct correlation with the catalyst concentration, resulting in bigger values of F , while the increment in variance extracted from the histograms means longer size distribution, as observed in nanotube thickness.

The TGA analysis was used to check the weight loss and the decomposition temperature of the as-prepared MWCNT. The results of this analysis are shown in Table 1. A direct

Table 1. Thermogravimetry Parameters of the As-Prepared MWCNT

	weight loss [%]	decomposition temp [°C]
2 wt %	96.1	663.0
5 wt %	94.2	643.9
10 wt %	87.6	611.7

dependence between the ferrocene content, used during the synthesis, the weight loss, and decomposition temperature is observed, confirming the previous statistical analysis performed.

According to the tip-growth mechanism during floating catalyst synthesis, it is very likely for the catalyst particle to be embedded within nanotubes. The amount and length of the particles can be directly controlled by increasing the amount of catalyst during the synthesis, as previously shown in this article, while keeping other grown parameters constant. It has been shown that the weight loss above 600 °C in samples containing iron particles correlates directly with its decomposition from metallic Fe into FeOx.^{19,37,38} This scenario is congruent with our observation and correlates with the higher ferrocene catalyst used in the reaction. Moreover, the decomposition temperature decreases for the samples with the higher ferrocene concentration. This couples with the nanoparticle decomposition effect and also suggests a decrement in the quality of nanotubes, i.e., graphitization degree.

Length Separation. The statistics of the length of O-MWCNT/iron hybrids after separation protocols were performed and studied by SEM. Micrographs were analyzed by ImageJ and B-spline fitting. A droplet of O-MWCNT dispersed in deionized water was placed on a SEM coverslip and subsequently dried by a membrane pump in a desiccator bell. SEM images of O-MWCNT for 5 wt % of catalyst, are shown as an example in Figure 4.

The direct influence of sonication speed (rpm) on the MWCNT length is observed. It is expected that the higher the centrifugation speed, the smaller the suspended nanotubes on the floating fluid. This clear difference can be only appreciated between 4000 and 8000 rpm, while histograms at 6000 rpm show not efficient size separation. It is useful to represent the length of the nanotubes, as the central peak of the normal distribution, including the reduced size distribution, that corresponds to the full width half-maximum (fwhm) of the

plot. These images are shown in Figure 5; long error bars are the result of partial superposition of nanotubes and in the case of values for 6000 rpm to a transitory step between both separation processes. It is important to remark that the bigger concentration of catalyst seems not to have mayor influence on the nanotubes length after centrifugation.

Quality Studies. Raman spectroscopy is a very useful technique to characterize the structure of carbon materials.^{39–41} Three basic modes—G (tangential stretching mode: 1500–1600 cm⁻¹), D (double-resonance mode: 1350 cm⁻¹), and RBM mode (radial breathing mode: 100–400 cm⁻¹)—are characteristic to SWCNT, MWCNT, and many different carbon structures.⁴² The D mode can be understood as a measurement of the structural disorders caused by acid treatment, e.g., some defects on the outer walls of MWCNT as well as the presence of amorphous carbon. The G mode originates from the tangential in plane stretching vibrations of the C–C bond within the graphene structure.⁴³ The disorder density of the CNT walls can be checked using the I_D/I_G ratio, where I_D and I_G are the areas (integral intensities) of the D and G peaks, respectively, obtained from the fitting of the spectra. The I_D/I_G ratio can be used to estimate the defect density of the nanotube outer walls. The smaller the I_D/I_G ratio, the fewer defects within the nanotubes.⁴⁴ Structural changes caused by the functionalization process are evident in spectra presented in Figure 6. The value of the I_D/I_G ratio between 0.59 and 0.70 confirms that the initial conditions of as-prepared MWCNT are coterminous.

During functionalization processes defects or functional groups are created on the outer walls of the MWCNT. Figure 7 presents I_D/I_G ratios of fractionated O-MWCNT using three different functionalization protocols described above. It is worth noticing the apparent influence of nanotubes length on the intensity of measured defects in the I_D/I_G ratio. This effect appears due to the increment in intensity of the D resonant mode for shorter MWCNT lengths. It is known, however, that the I_D/I_G ratio has some limitations, and its interpretation is somehow more a qualitative depiction of the nanotubes than a straightforward quality measure. The fundamental similarity in oxidative state of the measured nanotubes, which main difference is the length, allows us to perform a more unconventional quality ratio calculation based on the G' resonant mode, by calculating the $I_{G'}/I_D$ ratio Figure 7d.⁴⁵ It is clear that the increment on purity on MWCNT is observed for longer nanotubes. This observation is counterintuitive, since it is expected that the longer centrifugation processes and extra washing with deionized water that shorter nanotubes undergo will increment their purity. However, this is not the case. In our case, it is observed that longer nanotubes suffer less damage from the repetitive centrifugation process than short ones, showing a detriment on quality of O-MWCNT with each consecutive sonication and centrifugation process. Concordant with this observation is the fact that that sonication protocol is found to be the successfully oxidative process to the MWCNT.

Infrared spectroscopy can be used to extract information about independent chemical groups that are attached to the MWCNT. Compared to Raman spectroscopy, in which it is possible to estimate the extent of damages on the outer walls of O-MWCNT, FTIR spectroscopy can specify their nature. Figure 8 shows the infrared spectra of O-MWCNT with the same content of catalyst (5 wt %) and length for the three different oxidation protocols. The band labeled as (A) in the range of 3044–3712 cm⁻¹ is related to the vibration of the

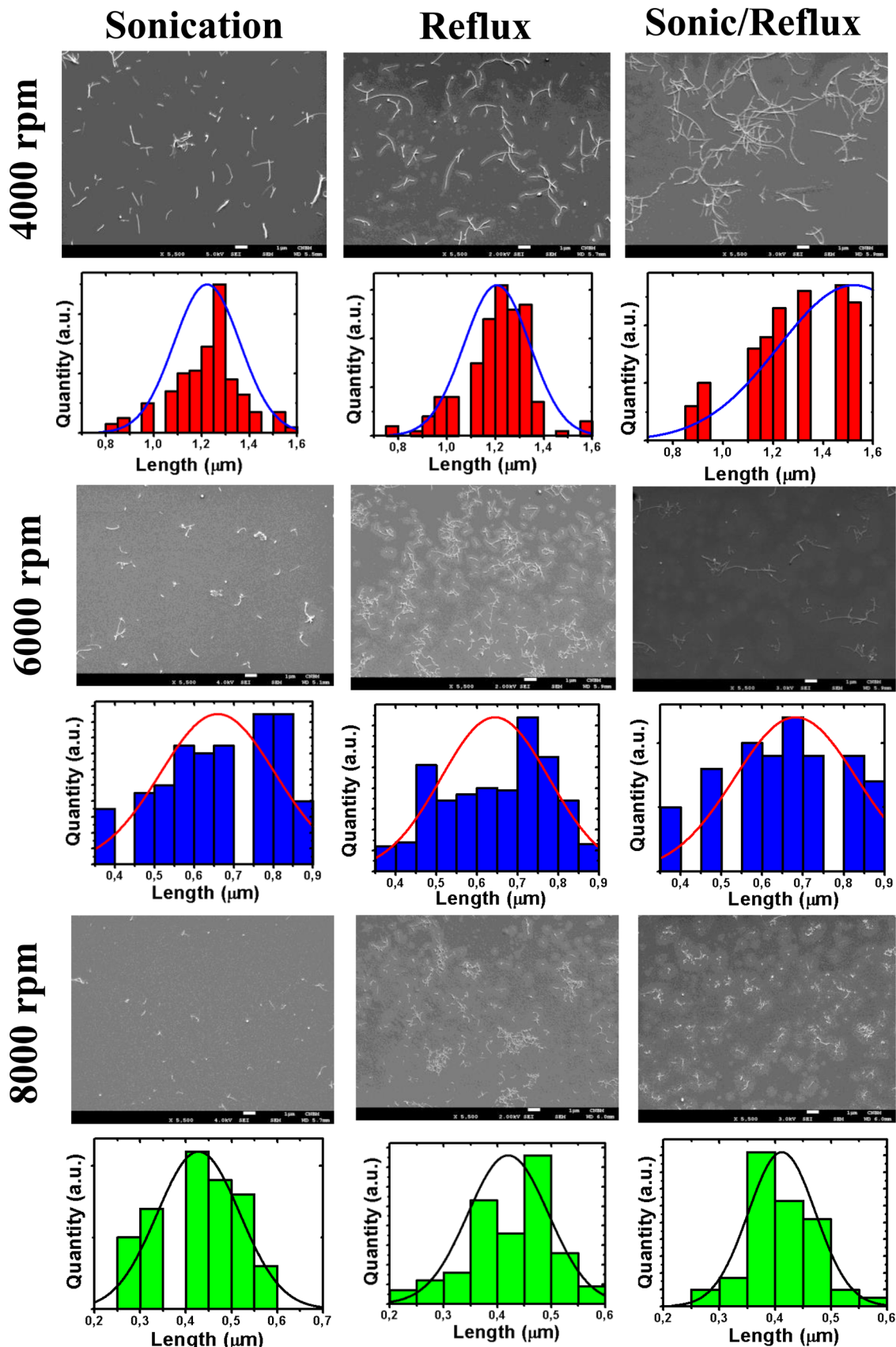


Figure 4. SEM micrographs of O-MWCNT (5 wt %) separated by centrifugation of speeds 4000, 6000, and 8000 rpm. Histograms show the length distribution observed after each process.

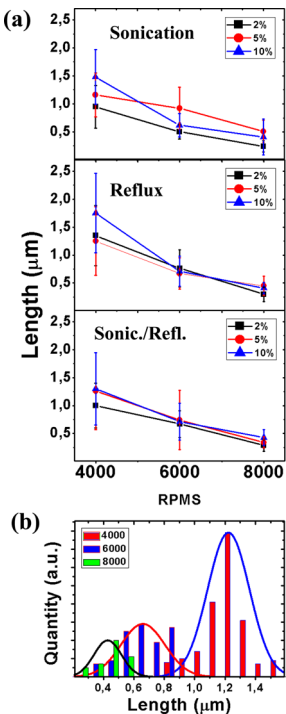


Figure 5. (a) Length distribution after size separation for different functionalization protocols. Plots show the nanotubes length vs RPMs. Concentration is noted as (■) 2%, (●) 5% and (▲) 10%. (b) Combination of the results of separation histograms for 5 wt % nanotubes functionalized by sonication; notice the clear selective size tendency of the separations process.

–OH groups while the absorption band (B) at around 1735 cm^{-1} is assigned to C=O strength vibration within COOH groups.^{13,46} In our case this peak is shifted and appears in the range from 1725 to 1706 cm^{-1} which can be caused by increasing the abundance of carboxyl groups with the treatment time. The peaks observed in the range from 1564 cm^{-1} to 1577 – 1581 and 1630 cm^{-1} (C, D) are assigned to $-\text{C}=\text{C}-$ groups. Finally, the peak appearing in the range of 1388 cm^{-1} can be ascribed to C–H within hydroxyl groups. According to FT-IR spectra for all separated by length O-MWCNT,

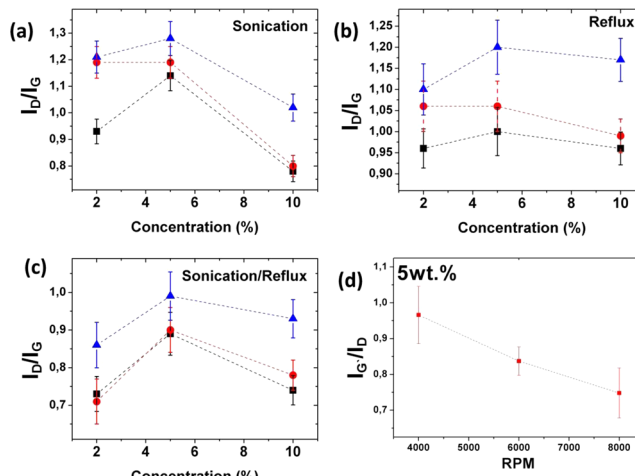


Figure 7. Values of $I_{\text{D}}/I_{\text{G}}$ ratio of the fractionated O-MWCNT for (a) sonication, (b) reflux, and (c) sonication/reflux. (d) $I_{\text{G}}/I_{\text{D}}$ ratio for the 5 wt % after separation protocol.

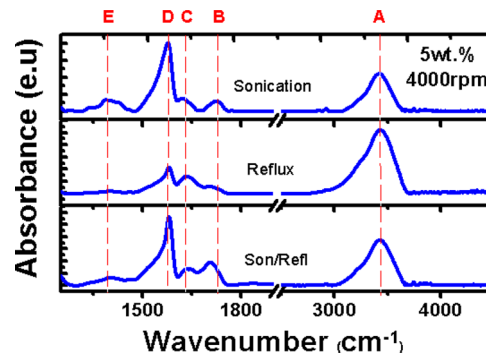


Figure 8. FTIR spectra of O-MWCNT with the same length, and different types of oxidation treatment: (A) –OH, (B) C=O, (C, D) –C=C–, (E) C–H.

sonication protocol is the most efficient at carboxyl and carbonyl group generation.

The HR-TEM technique was used to examine the quality of the obtained O-MWCNT. The micrograph shown in Figure 9

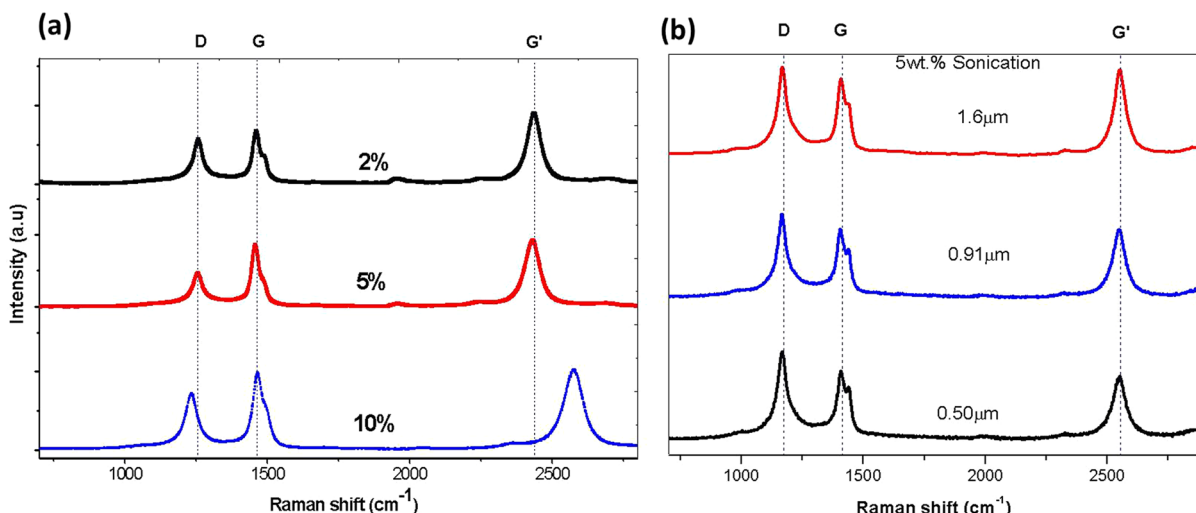


Figure 6. Raman spectra of (a) as-prepared MWCNT carpets with 2, 5, and 10 wt % content of catalyst. (b) The D, G, and G' modes of samples after the sonication oxidation protocol for sample: 5 wt % (4000, 6000, and 8000 rpm from top to down).

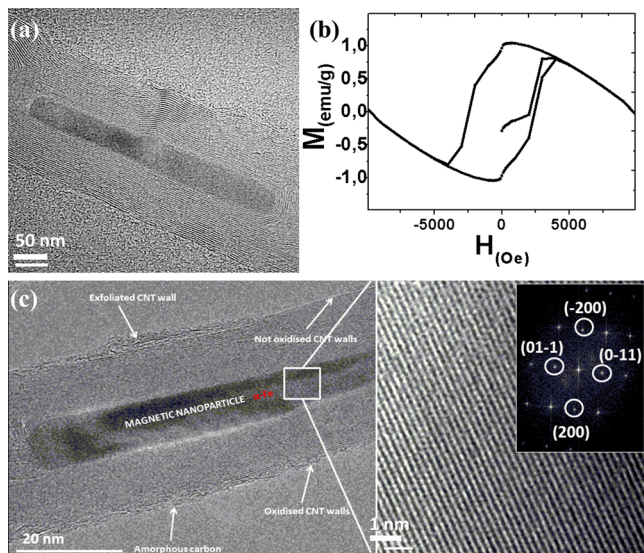


Figure 9. (a) HR-TEM micrographs of as-prepared 5 wt % MWCNT/ α -Fe composites. (b) Magnetic measurements performed at room temperature showing the magnetic nature of the samples. (c) HR-TEM image of 5 wt % MWCNT after sonication process. Notice that FFT extracted from HR-TEM images show clear features of α -Fe nanocrystals after functionalization procedures.

corresponds to O-MWCNT (4000 rpm, sonication) with 5 wt % of catalyst and confirms the presence of disorder on the outermost wall of the MWCNT as well as amorphous carbon after oxidation treatment, a feature not observed in as obtained nanotubes. High-resolution analysis of MWCNT/Fe composites confirms the highly crystalline nature of particles embedded in the nanotubes. Moreover, the fast Fourier transform diffraction pattern (FFT), using the (011) zone axis, unequivocally matches the unit cell of α -Fe (ferrite) (inset in Figure 9c) and account for the magnetization observed at room temperature of the composites (Figure 9b).

Hysteresis loops show a typical negative slope component, coupled with the hysteretic contribution of the α -Fe particles. This is a typical behavior of magnetic contributions, coupled with a diamagnetic media, in our case MWCNT account for the diamagnetism, while ferrite particles account for the ferromagnetism.⁴⁷ Remarkably enough, particles suffer no perceptible oxidation or damage during the functionalization process.

Stability. Water solutions containing functionalized MWCNT separated by multiple methods were stored at room temperature, under environmental conditions and room illumination, for a period of 4 months. Samples showed no visible segregation or agglomeration, and HR-TEM Figure 10a shows indistinguishable changes in morphology and dispersion between as-prepared samples and long-term stored. Moreover, FTIR (Figure 10b) spectra also confirmed stability of the functionalization procedure with no important changes in functional composition. Four major types of OH stretching modes can be present in FTIR spectra for water-based solutions. The spectral range of their location is between 3050 and 3720 cm^{-1} . Depending on their abundance and experiment conditions, they can coincide differently.^{48,49} The only noticeable differences between FT-IR spectra of long stored samples and freshly separated ones (Figure 10) are in the range of 3000–3600 cm^{-1} . Those peaks correspond to the hydrogen resonant modes. The apparition of obvious splitting

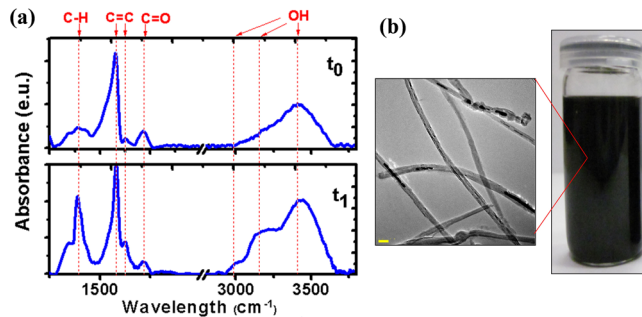


Figure 10. (a) FTIR spectra of O-MWCNT labeled t_0 and t_1 after 4 months in water suspension. (b) HR-TEM image and picture of the stable solution as seen after 4 months in uncontrolled storage.

after 4 months of storage implies the existence of three different populations which origin is under thorough study and analysis.

Further studies are being carried out regarding magnetic properties of O-MWCNT/ α -Fe solutions and powders, cytotoxic characterization, and in-situ NMR.

CONCLUSION AND FINAL REMARKS

Carbon nanotubes were synthesized using floating catalyst chemical vapor deposition method (FCCVD) with different concentrations of catalyst (ferrocene). A high quality carpet of aligned nanocomposite, nanotubes–magnetic particles, was obtained, and the influence of catalyst concentration on the morphology of the composites discussed. MWCNT were successfully functionalized by three different oxidation methods that showed different effect on the quality of the structures as shown by Raman and FTIR. Obtained nanotubes were separated by a simplified centrifugation protocol allowing the efficiently segregation method by length with a maximum size of 1.2 μm and minimum 0.3 μm . Nanocomposites showed excellent stability in water and the embedded nanoparticles do not suffer from oxidation or phase transformation due to functionalization procedures. Composites are stable in water over time, and their functional properties remain unchanged.

Finally, our study showed a reliable and reproducible way of single step synthesis of nanocomposites MWCNT/ α -Fe with excellent solubility and stability. The obtained results open exiting potential application as novel contrast agents, drug delivery systems, and magnetically controlled water-soluble environmental agents.

ASSOCIATED CONTENT

Supporting Information

Experimental details; Figures S1–S3. This material is available free of charge via the Internet at <http://pubs.acs.org>.

AUTHOR INFORMATION

Corresponding Author

* (B.M.M.): e-mail bmacieje@amu.edu.pl, phone +48618295239.

Notes

The authors declare no competing financial interest.

ACKNOWLEDGMENTS

L. E. Coy thanks the valuable discussions and collaboration of Dr. L. Yate from CIC biomaGUNE and Prof. Edgar Gonzales from Nanocitec. Financial support from the National Centre for Research and Development under research grant “Nano-

materials and Their Application to Biomedicine”, Contract PBS1/A9/13/2012, is gratefully acknowledged.

■ REFERENCES

- (1) Kis, A.; Zettl, A. Nanomechanics of Carbon Nanotubes. *Philos. Trans. R. Soc., A* **2008**, *366*, 1591–1611.
- (2) Kostarelos, K.; Bianco, A.; Prato, M. Promises, Facts and Challenges for Carbon Nanotubes in Imaging and Therapeutics. *Nat. Nanotechnol.* **2009**, *4*, 627–633.
- (3) Janas, D.; Koziol, K. K. Rapid Electrothermal Response of High-Temperature Carbon Nanotube Film Heaters. *Carbon* **2013**, *59*, 457–463.
- (4) Faraj, A. A.; Cieslar, K.; Lacroix, G. In Vivo Imaging of Carbon Nanotube Biodistribution Using Magnetic Resonance Imaging. *Nano Lett.* **2009**, *9*, 1023–1027.
- (5) Wick, P.; Manser, P.; Limbach, L. K.; Dettlaff-Weglowska, U.; Krumelich, F.; Roth, S.; Stark, W. J.; Bruinink, A. The Degree and Kind of Agglomeration Affect Carbon Nanotube Cytotoxicity. *Toxicol. Lett.* **2007**, *168*, 121–131.
- (6) Mukherjee, S.; Gupta, R.; Garg, A.; Bansal, V.; Bhargava, S. Influence of Zr Doping on the Structure and Ferroelectric Properties of BiFeO_3 Thin Films. *J. Appl. Phys.* **2010**, *107*, 123535.
- (7) Sohaebuddin, S. K.; Thevenot, P. T.; Baker, D.; Eaton, J. W.; Tang, L. Nanomaterial Cytotoxicity Is Composition, Size, and Cell Type Dependent. *Part. Fibre Toxicol.* **2010**, *7*, 22.
- (8) Smart, S. K.; Cassady, A. I.; Lu, G. Q.; Martin, D. J. The Biocompatibility of Carbon Nanotubes. *Carbon* **2006**, *44*, 1034–1047.
- (9) Ren, J.; Shen, S.; Wang, D.; Xi, Z.; Guo, L.; Pang, Z.; Qian, Y.; Sun, X.; Jiang, X. The Targeted Delivery of Anticancer Drugs to Brain Glioma by PEGylated Oxidized Multi-Walled Carbon Nanotubes Modified with Angiopep-2. *Biomaterials* **2012**, *33*, 3324–3333.
- (10) Shi Kam, N. W.; Jessop, T. C.; Wender, P. A.; Dai, H. Nanotube Molecular Transporters: Internalization of Carbon Nanotube-Protein Conjugates into Mammalian Cells. *J. Am. Chem. Soc.* **2004**, *126*, 6850–6851.
- (11) Nagai, H.; Okazaki, Y.; Chew, S. H.; Misawa, N.; Yamashita, Y.; Akatsuka, S.; Ishihara, T.; Yamashita, K.; Yoshikawa, Y.; Yasui, H.; et al. Diameter and Rigidity of Multiwalled Carbon Nanotubes Are Critical Factors in Mesothelial Injury and Carcinogenesis. *Proc. Natl. Acad. Sci. U. S. A.* **2011**, *108*, E1330–8.
- (12) Chen, J. Solution Properties of Single-Walled Carbon Nanotubes. *Science* **1998**, *282*, 95–98.
- (13) Datsyuk, V.; Kalyva, M.; Papagelis, K.; Parthenios, J.; Tasis, D.; Siokou, A.; Kallitsis, I.; Galiotis, C. Chemical Oxidation of Multiwalled Carbon Nanotubes. *Carbon* **2008**, *46*, 833–840.
- (14) Cheng, F.-Y.; Su, C.-H.; Yang, Y.-S.; Yeh, C.-S.; Tsai, C.-Y.; Wu, C.-L.; Wu, M.-T.; Shieh, D.-B. Characterization of Aqueous Dispersions of Fe_3O_4 Nanoparticles and Their Biomedical Applications. *Biomaterials* **2005**, *26*, 729–738.
- (15) Jun, Y.-W.; Seo, J.-W.; Cheon, J. Nanoscaling Laws of Magnetic Nanoparticles and Their Applicabilities in Biomedical Sciences. *Acc. Chem. Res.* **2008**, *41*, 179–189.
- (16) Mahmoudi, M.; Serpooshan, V.; Laurent, S. Engineered Nanoparticles for Biomolecular Imaging. *Nanoscale* **2011**, *3*, 3007–3026.
- (17) Renshaw, P. F.; Owen, C. S.; McLaughlin, A. C.; Frey, T. G.; Leigh, J. S. Ferromagnetic Contrast Agents: A New Approach. *Magn. Reson. Med.* **1986**, *3*, 217–225.
- (18) Koenig, S. H.; Kellar, K. E. Theory of 1/T1 and 1/T2 NMRD Profiles of Solutions of Magnetic Nanoparticles. *Magn. Reson. Med.* **1995**, *34*, 227–233.
- (19) Zhao, X.; Xia, D.; Zheng, K. $\text{Fe}_3\text{O}_4/\text{Fe}/\text{Carbon}$ Composite and Its Application as Anode Material for Lithium-Ion Batteries. *ACS Appl. Mater. Interfaces* **2012**, *4*, 1350–1356.
- (20) Choi, J. H.; Nguyen, F. T.; Barone, P. W.; Heller, D. A.; Moll, A. E.; Patel, D.; Boppert, S. A.; Strano, M. S. Multimodal Biomedical Imaging with Asymmetric Single-Walled Carbon Nanotube/Iron Oxide Nanoparticle Complexes. *Nano Lett.* **2007**, *7*, 861–867.
- (21) Ananta, J. S.; Matson, M. L.; Tang, A. M.; Mandal, T.; Lin, S.; Wong, K.; Wong, S. T.; Wilson, L. J. Single-Walled Carbon Nanotube Materials as T 2-Weighted MRI Contrast Agents. *J. Phys. Chem. C* **2009**, *113*, 19369–19372.
- (22) Vittorio, O.; Duce, S. L.; Pietrabissa, A.; Cuschieri, A. Multiwall Carbon Nanotubes as MRI Contrast Agents for Tracking Stem Cells. *Nanotechnology* **2011**, *22*, 095706.
- (23) Yin, M.; Wang, M.; Miao, F.; Ji, Y.; Tian, Z.; Shen, H.; Jia, N. Water-Dispersible Multiwalled Carbon Nanotube/Iron Oxide Hybrids as Contrast Agents for Cellular Magnetic Resonance Imaging. *Carbon* **2012**, *50*, 2162–2170.
- (24) Liu, Y.; Hughes, T. C.; Muir, B. W.; Waddington, L. J.; Gengenbach, T. R.; Easton, C. D.; Hinton, T. M.; Moffat, B. A.; Hao, X.; Qiu, J. Water-Dispersible Magnetic Carbon Nanotubes as T2-Weighted MRI Contrast Agents. *Biomaterials* **2014**, *35*, 378–386.
- (25) Wang, J. T.-W.; Cabana, L.; Bourgognon, M.; Kafa, H.; Protti, A.; Venner, K.; Shah, A. M.; Sosabowski, J. K.; Mather, S. J.; Roig, A.; et al. Magnetically Decorated Multiwalled Carbon Nanotubes as Dual MRI and SPECT Contrast Agents. *Adv. Funct. Mater.* **2014**, *24*, 1880–1894.
- (26) Liu, Z.; Yang, K.; Lee, S.-T. Single-Walled Carbon Nanotubes in Biomedical Imaging. *J. Mater. Chem.* **2011**, *21*, 586.
- (27) Wu, H.; Liu, G.; Wang, X.; Zhang, J.; Chen, Y.; Shi, J.; Yang, H.; Hu, H.; Yang, S. Solvothermal Synthesis of Cobalt Ferrite Nanoparticles Loaded on Multiwalled Carbon Nanotubes for Magnetic Resonance Imaging and Drug Delivery. *Acta Biomater.* **2011**, *7*, 3496–3504.
- (28) Koziol, K.; Boskovic, B.; Yahya, N. *Synthesis of Carbon Nanostructures by CVD Method*; Advanced Structured Materials; Springer: Berlin, 2011; Vol. 5, pp 23–49.
- (29) Kumar, M.; Ando, Y. Chemical Vapor Deposition of Carbon Nanotubes: A Review on Growth Mechanism and Mass Production. *J. Nanosci. Nanotechnol.* **2010**, *10*, 3739–3758.
- (30) Liu, J. Fullerene Pipes. *Science* **1998**, *280*, 1253–1256.
- (31) Vinciguerra, V.; Buonocore, F. Growth Mechanisms in Chemical Vapour Deposited Carbon Nanotubes. *Nanotechnology* **2003**, *14*, 655–660.
- (32) Weissker, U.; Hampel, S.; Leonhardt, A.; Büchner, B. Carbon Nanotubes Filled with Ferromagnetic Materials. *Materials (Basel)* **2010**, *3*, 4387–4427.
- (33) Xu, J. Y.; Lei, X. C.; Yang, R.; Fan, Z. Z. In Situ Formation of Carbon Nanomaterials on Bulk Metallic Materials. *J. Nanomater.* **2014**, *2014*, 1–9.
- (34) Kunadian, I.; Andrews, R.; Qian, D.; Pinar Mengüç, M. Growth Kinetics of MWCNTs Synthesized by a Continuous-Feed CVD Method. *Carbon* **2009**, *47*, 384–395.
- (35) Müller, C.; Hampel, S.; Elefant, D.; Biedermann, K.; Leonhardt, A.; Ritschel, M.; Büchner, B. Iron Filled Carbon Nanotubes Grown on Substrates with Thin Metal Layers and Their Magnetic Properties. *Carbon* **2006**, *44*, 1746–1753.
- (36) Wang, W.; Wang, K.; Lv, R.; Wei, J.; Zhang, X. Synthesis of Fe-Filled Thin-Walled Carbon Nanotubes with High Filling Ratio by Using Dichlorobenzene as Precursor. *Carbon* **2007**, *45*, 1127–1129.
- (37) Kim, J.; Chung, M. K.; Ka, B. H.; Ku, J. H.; Park, S.; Ryu, J.; Oh, S. M. The Role of Metallic Fe and Carbon Matrix in $\text{Fe}_3\text{O}_4/\text{Fe}/\text{Carbon}$ Nanocomposite for Lithium-Ion Batteries. *J. Electrochem. Soc.* **2010**, *157*, A412.
- (38) Burke, N.; Stöver, H.; Dawson, F. Magnetic Nanocomposites: Preparation and Characterization of Polymer-Coated Iron Nanoparticles. *Chem. Mater.* **2002**, *14*, 4752–4761.
- (39) Osswald, S.; Havel, M.; Gogotsi, Y. Monitoring Oxidation of Multiwalled Carbon Nanotubes by Raman Spectroscopy. *Raman Spectrosc.* **2007**, *728–736*.
- (40) Jorio, A.; Saito, R.; Dresselhaus, G.; Dresselhaus, M. S. Determination of Nanotubes Properties by Raman Spectroscopy. *Philos. Trans. R. Soc., A* **2004**, *362*, 2311–2336.
- (41) Dresselhaus, M. S.; Dresselhaus, G.; Saito, R.; Jorio, A. Raman Spectroscopy of Carbon Nanotubes. *Phys. Rep.* **2005**, *409*, 47–99.

- (42) Thomsen, C.; Reich, S.; Maultzsch, J. Resonant Raman Spectroscopy of Nanotubes. *Philos. Trans. R. Soc., A* **2004**, *362*, 2337–2359.
- (43) Singh, C.; Shaffer, M.; Windle, A. Production of Controlled Architectures of Aligned Carbon Nanotubes by an Injection Chemical Vapour Deposition Method. *Carbon* **2003**, *41*, 359–368.
- (44) Lehman, J. H.; Terrones, M.; Mansfield, E.; Hurst, K. E.; Meunier, V. Evaluating the Characteristics of Multiwall Carbon Nanotubes. *Carbon* **2011**, *49*, 2581–2602.
- (45) DiLeo, R. A.; Landi, B. J.; Raffaelle, R. P. Purity Assessment of Multiwalled Carbon Nanotubes by Raman Spectroscopy. *J. Appl. Phys.* **2007**, *101*, 064307.
- (46) Zhang, J.; Zou, H.; Qing, Q.; Yang, Y.; Li, Q.; Liu, Z.; Guo, X.; Du, Z. Effect of Chemical Oxidation on the Structure of Single-Walled Carbon Nanotubes. *J. Phys. Chem. B* **2003**, *107*, 3712–3718.
- (47) Dresselhaus, M. S.; Dresselhaus, G.; Saito, R. Physics of Carbon Nanotubes. *Carbon* **1995**, *33*, 883–891.
- (48) Byl, O.; Liu, J.; Wang, Y.; Yim, W.; Johnson, J. K.; Yates, J. T.; Chemie, A.; Carl, V.; Uni, O.; Str, C.-V.; et al. Unusual Hydrogen Bonding in Water-Filled Carbon Nanotubes. *J. Am. Chem. Soc.* **2006**, 12090–12097.
- (49) NathanieláPribble, R. Probing Hydrogen Bonding in Benzene–(Water) N Clusters Using Resonant Ion-Dip IR Spectroscopy. *Faraday Discuss.* **1994**, 229–241.
- (50) Maciejewska, B. M.; Jasurkowska-Delaporte, M.; Vasylenko, A. I.; Koziol, K. K.; Jurga, S. Experimental and Theoretical Studies on the Mechanism for Chemical Oxidation of Multiwalled Carbon Nanotubes. *RSC Adv.* **2014**, *4*, 28826.